Check for updates

Wiley
International Journal of Energy Research
Volume 2024, Article ID 3192642, 14 pages
https://doi.org/10.1155/2024/3192642

WILEY

Research Article

Synthesis of MoS_2/WS_2 Nanoflower Heterostructures for Hydrogen Evolution Reaction

Tuan Van Nguyen,[1] **Mahider Tekalgne**,[1] **Chau Van Tran**,[2] **Thang Phan Nguyen**,[3] **Vandung Dao**,[4] **Quyet Van Le**,[1] **Sang Hyun Ahn**,[5] **and Soo Young Kim**[1]

[1]*Department of Materials Science and Engineering, Institute of Green Manufacturing Technology, Korea University, 145 Anam-ro, Seoul 02841, Seongbuk-gu, Republic of Korea*
[2]*Advanced Technology Center, Le Quy Don Technical University, 236 Hoang Quoc Viet, Hanoi 11917, Vietnam*
[3]*Department of Chemical and Biological Engineering, Gachon University, Seongnam-si 13120, Gyeonggi-do, Republic of Korea*
[4]*Department of Materials Science and Engineering, Korea University, Seoul 02841, Republic of Korea*
[5]*School of Chemical Engineering and Materials Science, Chung-Ang University, 84 Heukseok-ro, Seoul 06974, Dongjak-gu, Republic of Korea*

Correspondence should be addressed to Sang Hyun Ahn; shahn@cau.ac.kr and Soo Young Kim; sooyoungkim@korea.ac.kr

Received 23 February 2024; Revised 24 April 2024; Accepted 4 July 2024

Academic Editor: Juan M. Coronado

Copyright © 2024 Tuan Van Nguyen et al. This is an open access article distributed under the Creative Commons Attribution License, which permits unrestricted use, distribution, and reproduction in any medium, provided the original work is properly cited.

Over the last decades, the transition metal dichalcogenide (TMD) materials have been intensively investigated for hydrogen evolution reaction (HER). Among many TMD catalysts, MoS_2 and WS_2 are the most efficient materials for HER application because of their advantages including earth abundance, facile synthesis, and high catalytic activities. Herein, a simple and scalable process is introduced which was employed to prepare the nanoflower (NF) heterostructure of MoS_2 and WS_2 (MoS_2/WS_2 NF). The superior catalytic activity of the synthesized MoS_2/WS_2 NF could be contributed by the unique properties of the heterostructure between WS_2 and MoS_2 materials. Low overpotential (251 mV) at a current density of 10 mA cm^{-2}, small Tafel slope (61 mV dec^{-1}), good conductivity, and superstability are the main properties of the prepared MoS_2/WS_2 NF. This work presents a new facile novel to prepare efficient catalysts which could be great candidates for HER and electrocatalytic application.

1. Introduction

Over the last decades, along with the development of high technologies and the increasing demand for ecofriendly and renewable energy, various approaches and materials applied for different technologies have been extensively investigated such as perovskite quantum dot materials [1, 2], photoelectrochemical processes [3, 4, 5, 6, 7, 8], CO_2 reduction [9], electrochromic window [10], solar water splitting [11], and electrocatalysts [12]. Among them, hydrogen technology is considered as the most promising answer for different areas such as transportation, heat cooling energy, power energy, and fertilizer because of its advantages [13, 14, 15, 16, 17]. To produce hydrogen, there are also a number of processes which could be applied to harvest the released hydrogen gases [18, 19, 20, 21, 22]. To date, electrochemical process or electrolysis of water technique has been evaluated as the most simple and effective method to prepare hydrogen gas. In water splitting process, the hydrogen gas could be released from the surface of cathode electrode. Therefore, the quantity of the produced hydrogen gas is highly depended on the properties of materials which are employed to prepare cathode electrode. For that reason, the better the catalytic activity of cathode electrode, the higher the yield of hydrogen gas could be produced. In the past, the hydrogen gases are usually prepared by using the noble metal cathode such as platinum or palladium materials. The high catalytic activity and low hydrogen biding energy are the key advantages of those noble metals [23, 24, 25]. However, the scarcity, unstability, and expensive materials of noble metals are the main drawbacks which are needed to overcome [26, 27, 28]. Consequently, a low-cost, stable, and efficient catalysts for HER process are the main target for hydrogen energy technologies in large-scale and practical technologies.

Table 1: Materials for synthesis of MoS_2/WS_2 NF, MoS_2 NF, and WS_2 NF.

No.	AMH (g)	AMT (g)	TAA (g)	H_2O (mL)	NH_3 (mL)	HCl (mL)	t (°C)	Catalysts
1	2	1.3	5	15	0	3	220	MoS_2/WS_2 NF
2	4	0	5	18	0	0	220	WS_2 NF
3	0	2.6	5	15	3	0	220	MoS_2 NF

Recently, transition metal dichalcogenide (TMD) materials have been emerging as prominent catalysts which could be applied for HER process because of their low-cost, super stable, and high catalytic activity toward electrochemical application. Among many TMD catalysts, WS_2 and MoS_2 are being considered as alternative materials for noble metals in hydrogen production process. They possess fascinating electronic properties, with both MoS_2 and WS_2 being a semiconductor with a indirect bandgap, while their respective monolayers exhibit direct electronic bandgaps [29, 30, 31, 32]. Recently, considerable efforts have been devoted to maximize and optimize the catalytic activities of catalysts based on WS_2 and MoS_2 materials. Different morphologies, structures, or derivatives of catalysts based on WS_2 and MoS_2 have been prepared and studied [33, 34, 35]. Many reports have indicated that the catalytic performance of catalysts based on the heterostructure of two or more materials could be dramatically boosted because of the synergistic effect or the unique properties of the prepared materials [36, 37, 38, 39]. Thus, the construction of a heterostructure through the integration of MoS_2 and WS_2 benefits from the favorable band alignment between the two materials, facilitating rapid charge transfer and ensuring high conductivity within the MoS_2/WS_2 heterostructure.

In this manuscript, a facile and scalable process which was applied to prepare nanoflower (NF) heterostructure of MoS_2 and WS_2: MoS_2/WS_2 NF. Besides that, the pure WS_2 NF and MoS_2 NF were also prepared by the same processes with slight modification. The structures and morphologies of synthesized materials were completely studied to compare and understand the difference between them. After that, the electrocatalytic activities of MoS_2/WS_2 NF, WS_2 NF, and MoS_2 NF were also investigated for HER application. The results confirmed the HER performance of MoS_2/WS_2 NF has been significantly increased compared with that of WS_2 NF and MoS_2 NF. Therefore, MoS_2/WS_2 NF could be considered as a next generation of catalyst materials for HER and electrochemical applications.

2. Experimental

2.1. Chemicals. Ammonium metatungstate hydrate, $(NH_4)_6H_2W_{12}O_{40}{\cdot}xH_2O$ (AMH), ammonium molybdate tetrahydrate (AMT, $(NH_4)_6Mo_7O_{24}{\cdot}4H_2O$), thioacetamide (TAA, CH_3CSNH_2), HCl (37% aqueous solution), NH_3 (28% aqueous solution), and Nafion (5% aqueous solution) were purchased from Sigma–Aldrich. Deionized (DI) water was obtained from Millipore Mili-Q. All chemicals were used without further purification.

2.2. Synthesis of MoS_2/WS_2 NF. The synthesis processes were slightly modified compare with the previous study [13]. MoS_2/WS_2 NF material was synthesized via a facile one-step hydrothermal method. Appropriate amounts of AMH, AMT, TAA, and DI water were added to a glass beaker and stirred for 15 min. After that, an amount of HCl (37%) was added to the prepared mixture and continuously stirred for 15 min before transferring into a Teflon autoclave. The autoclave was heated to 220°C for 24 hr and then cooled down to room temperature. The synthesized catalyst was centrifuged at a speed of approximately 8,000 rpm using DI water and ethanol three times to eliminate all excessive components. After that, the catalyst was dried at 90°C and then annealed in inert gas to obtain MoS_2/WS_2 NF. The produced catalyst was stored in a glass vial for the next measurements. The pure WS_2 NF and MoS_2 NF were also synthesized via the same route with changing some source materials. The exact amounts of all source materials during syntheses are listed in Table 1.

2.3. Electrochemical Measurements. All electrochemical measurements were performed at room temperature using a standard three-electrode electrolytic system and Ivium potentiostat V55630. A saturated calomel electrode, graphite electrode, and the synthesized catalysts on glassy carbon electrodes were employed as the reference, counter, and working electrodes, respectively. The HER activities of MoS_2/WS_2 NF, WS_2 NF, and MoS_2 NF were evaluated via linear sweep voltammetry (LSV) at a scan rate of 10 mV s^{-1}. All measurements were conducted in a 0.5 M H_2SO_4 solution with an iR correction. The stability of MoS_2/WS_2 NF was examined by continuous cyclic voltammetry (CV) at a scan rate of 50 mV s^{-1} for over 1,000 cycles. Thereafter, the stability of the prepared MoS_2 SNFs was continuously evaluated via chronoamperometry (CA) for 12 hr. Double-layer capacitance (C_{dl}) values of the studied samples were calculated from the results of CV tests, which were performed in the potential range from 0 to 0.2 V at different scan rates (20, 40, 60, 80, and 100 mV s^{-1}). Additionally, electrochemical impedance spectroscopy (EIS) was conducted in a frequency range of 100 kHz to 0.1 Hz.

2.4. Characterization of MoS_2 NFs and SNFs. X-ray diffraction (XRD) was employed to examine the structures and crystallinities of the prepared MoS_2/WS_2 NF, WS_2 NF, and MoS_2 NF using a powder X-ray diffractometer with Cu Kα radiation ($\lambda = 0.154$ nm). The structures and chemical bonding of the prepared catalysts were investigated by Raman spectroscopy. X-ray photoelectron spectroscopy (XPS) was conducted to determine the surface compositions of the prepared MoS_2 SNF materials. Field emission scanning electron

ijer, 2024, 1, Downloaded from https://onlinelibrary.wiley.com/doi/10.1155/2024/3192642 by Chung-Ang University, Wiley Online Library on [13/08/2024]. See the Terms and Conditions (https://onlinelibrary.wiley.com/terms-and-conditions) on Wiley Online Library for rules of use; OA articles are governed by the applicable Creative Commons License

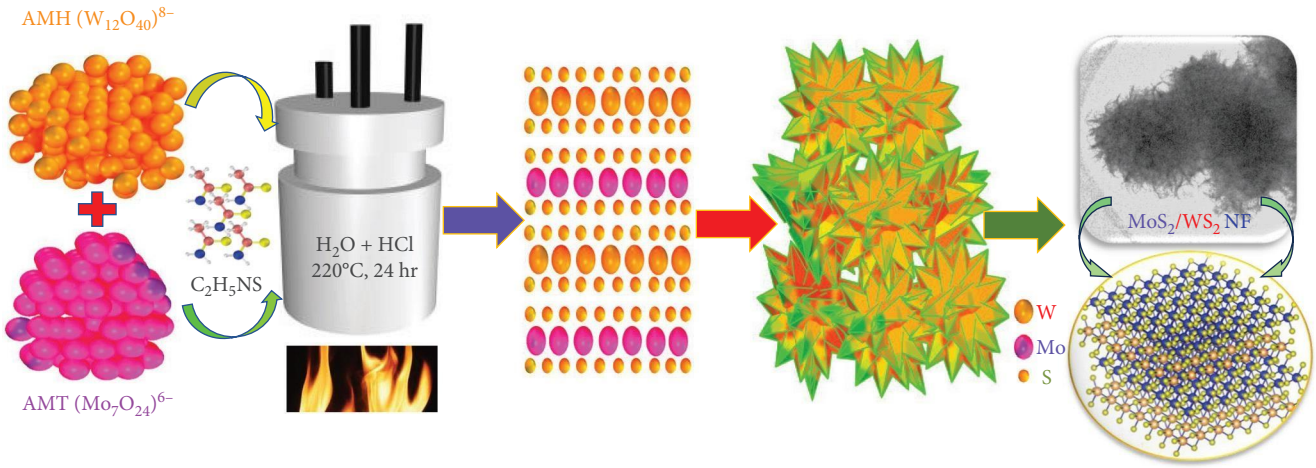


FIGURE 1: Proposed mechanism of MoS_2/WS_2 NF synthesis process.

microscopy (FE–SEM) was employed to comprehensively observe the morphology, size, and shape of the synthesized catalysts. Transmission electron microscopy (TEM) was utilized to determine the structure and elemental distributions on the material surfaces. The work function of catalysts could be calculated from ultraviolet photoelectron spectroscopy (UPS) measurements which were conducted by using UV source: He1 21.2 eV. Pore size, pore volume, and specific surface areas of the catalysts were calculated by the Brunauer–Emmett–Teller (BET) method from the adsorption–desorption of nitrogen gas on the surface of prepared catalysts.

3. Results and Discussion

3.1. Formation Mechanism of Synthesis Processes. The formation of MoS_2/WS_2 NF, WS_2 NF, and MoS_2 NF could be explained by followed reaction:

(1) The MoS_2/WS_2 NF synthesis process which is illustrated in Figure 1 is as follows:

$$HCl \rightarrow H^+ + Cl^-, \quad (1)$$

$$(NH_4)_6Mo_7O_{24} \cdot 4H_2O + H_2O \rightarrow 6NH_4^+ + [Mo_7O_{24}]^{6-} + 4H_2O, \quad (2)$$

$$[Mo_7O_{24}]^{6-} + 6H^+ \rightarrow 7MoO_3 + 3H_2O, \quad (3)$$

$$(NH_4)_6H_2W_{12}O_{40}.xH_2O \rightarrow 6NH_3 + 8H^+ + [W_{12}O_{40}]^{8-} + xH_2O, \quad (4)$$

$$[W_{12}O_{40}]^{8-} + 8H^+ \rightarrow 12WO_3 + 4H_2O, \quad (5)$$

$$CH_3CSNH_2 + 2H_2O \rightarrow NH_3 + H_2S + CH_3COOH, \quad (6)$$

$$3MoO_3 + 7H_2S \rightarrow 3MoS_2\downarrow + SO_2 + 7H_2O, \quad (7)$$

$$3WO_3 + 7H_2S \rightarrow 3WS_2\downarrow + SO_2 + 7H_2O. \quad (8)$$

(2) The WS_2 NF synthesis process is as follows:

$$(NH_4)_6H_2W_{12}O_{40}.xH_2O \rightarrow 6NH_3 + 8H^+ + [W_{12}O_{40}]^{8-} + xH_2O, \quad (9)$$

$$CH_3CSNH_2 + 2H_2O \rightarrow H_2S + NH_3 + H^+ + CH_3COO^-, \quad (10)$$

$$[W_{12}O_{40}]^{8-} + 8H^+ \rightarrow 12WO_3 + 4H_2O, \quad (11)$$

$$3WO_3 + 7H_2S \rightarrow 3WS_2\downarrow + SO_2 + 7H_2O. \quad (12)$$

(3) The MoS_2 NF synthesis process is as follows:

$$(NH_4)_6Mo_7O_{24} \cdot 4H_2O \rightarrow 6NH_4^+ + [Mo_7O_{24}]^{6-} + 4H_2O, \quad (13)$$

$$CH_3CSNH_2 + 2H_2O \rightarrow H_2S + NH_4^+ + CH_3COO^-, \quad (14)$$

$$NH_3 + H_2O \rightarrow NH_4^+ + OH^-, \quad (15)$$

$$[Mo_7O_{24}]^{6-} + 6NH_4^+ \rightarrow 7MoO_3 + 6NH_3 + 3H_2O, \quad (16)$$

$$3MoO_3 + 7H_2S \rightarrow 3MoS_2\downarrow + SO_2 + 7H_2O. \quad (17)$$

The crystallinity of the synthesized MoS_2/WS_2 NF, WS_2 NF, and MoS_2 NF is completely studied by XRD which are

ijer, 2024, 1, Downloaded from https://onlinelibrary.wiley.com/doi/10.1155/2024/3192642 by Chung-Ang University, Wiley Online Library on [13/08/2024]. See the Terms and Conditions (https://onlinelibrary.wiley.com/terms-and-conditions) on Wiley Online Library for rules of use; OA articles are governed by the applicable Creative Commons License

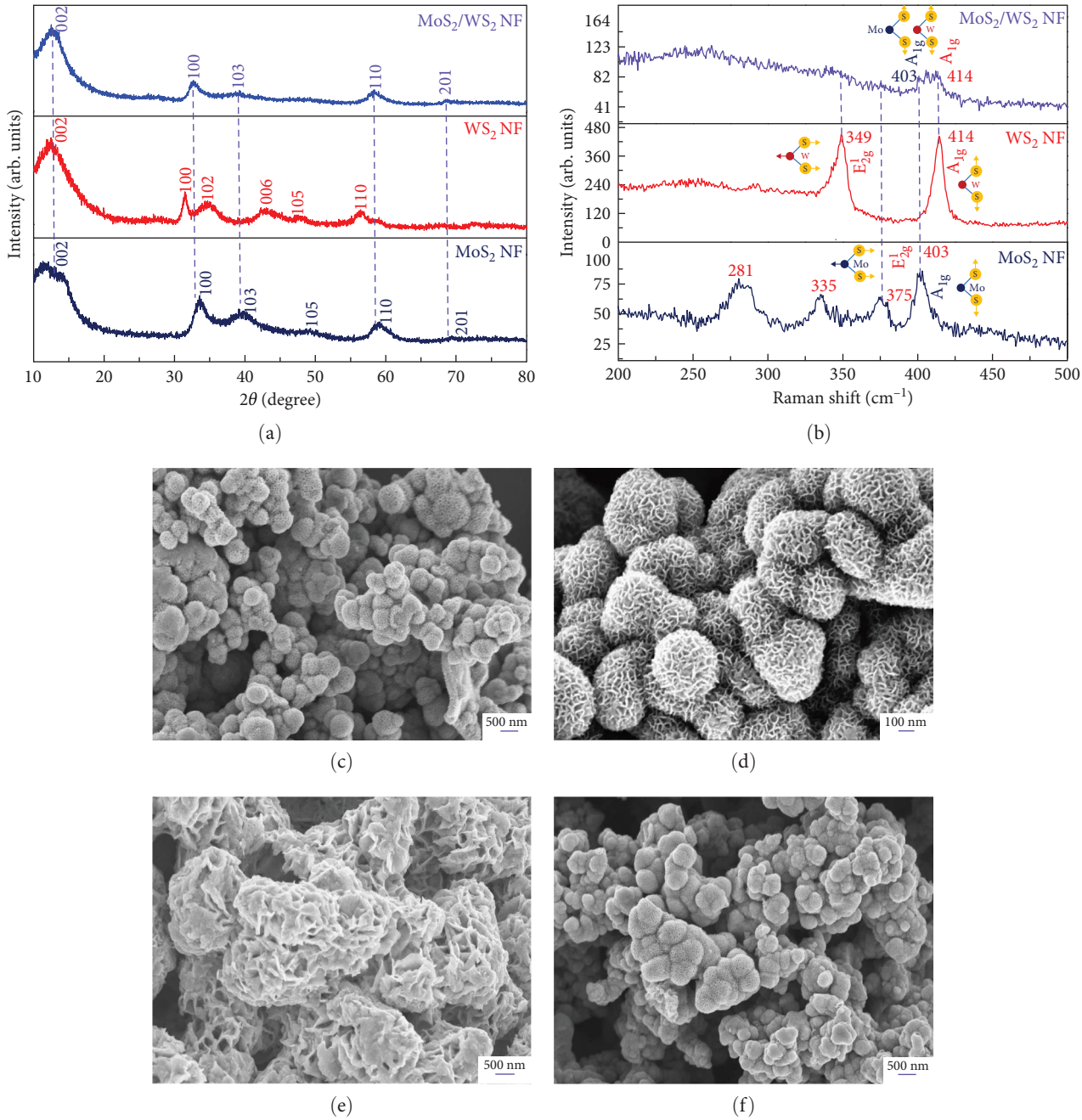


FIGURE 2: (a) XRD patterns of MoS_2/WS_2 NF, WS_2 NF, and MoS_2 NF materials; (b) Raman spectra of MoS_2/WS_2 NF, WS_2 NF, and MoS_2 NF materials; and FE-SEM images of (c), (d) MoS_2/WS_2 NF, (e) WS_2 NF, and (f) MoS_2 NF materials.

presented in Figure 2. In MoS_2 NF XRD patterns, there are six main peaks which are indexed as (002), (100), (0103), (105), (110), and (201) plane without any diffraction peaks from impurities of other parasitic phase. The XRD pattern indicates that highly pure hexagonal MoS_2 materials are successfully prepared which are in good agreement with the literature values (JCPDS: 00-037-1492) [40]. The XRD data of WS_2 NF also show six main peaks which are located at (002), (100), (102), (006), (105), and (110) plane. The XRD analysis of synthesized WS_2 shows high crystalline hexagonal structure which was reported in previous study (PDF no. 84-1398) without any other impurities [41]. Figure 2(a) also presents the XRD pattern of the prepared MoS_2/WS_2 NF. As can be seen, there are only five main peaks which are located at (002), (100), (103), (110), and (201) plane. Interestingly, those peaks are slightly shifted compared to the peaks of both synthesized WS_2 NF and MoS_2 NF. It could be assigned to the effect of interlayer or the disorder between MoS_2 and WS_2 layers. The XRD data indicate that the heterostructure MoS_2/WS_2 NF as well as WS_2 NF and MoS_2 NF materials are well prepared.

The Raman spectroscopy measurements are also conducted to investigate the atomic structure arrangement of the prepared MoS_2/WS_2 NF, WS_2 NF, and MoS_2 NF materials. Figure 2(b)

ijer, 2024, 1, Downloaded from https://onlinelibrary.wiley.com/doi/10.1155/2024/3192642 by Chung-Ang University, Wiley Online Library on [13/08/2024]. See the Terms and Conditions (https://onlinelibrary.wiley.com/terms-and-conditions) on Wiley Online Library for rules of use; OA articles are governed by the applicable Creative Commons License

show typical Raman spectra of the synthesized catalysts. As can be seen that the Raman spectrum of MoS_2 NF is dominated by two characteristic bands at 377 and 404 cm^{-1}. These bands are attributed to the in-plane E^1_{2g} mode (375 cm^{-1}) derived from opposite vibrations of two S atoms with respect to the Mo atom, the A_{1g} mode (403 cm^{-1}) associated with the out-of-plane vibration of S atoms [42]. Notably, the presence of two new bands centered at 281 and 335 cm^{-1} further justified formation of the 1T-MoS_2 phase in the synthesized material [43]. In the Raman spectra of WS_2 NF, the Raman spectrum is dominated by the two peaks located at around at 349 cm^{-1} (E^1_{2g}) and 414 cm^{-1} (A_{1g}) which are in line with previous reports [44, 45]. Similar with XRD patterns, the Raman spectrum of MoS_2/WS_2 NF has changed a little compared to that of pure WS_2 NF and MoS_2 NF materials. As can be seen, there are low-density peaks located at around 403 and 414 cm^{-1} which could be assigned to out-of-plane vibration of S atoms (A_{1g}) in Mo—S and W—S bonding, respectively. For others, the peaks of WS_2 and MoS_2 are not clearly observed. It indicated that the heterostructure of MoS_2/WS_2 NF could be formed [46].

The morphologies of the prepared MoS_2/WS_2 NF, WS_2 NF, and MoS_2 NF materials are completely studied by FE-SEM images. As can be seen from Figures 2(c) and 2(d), the morphology of MoS_2/WS_2 NF is highly similar with that of MoS_2 NF material Figure 2(e), and they are dramatically different from that of WS_2 NF materials Figure 2(f), which are significantly bigger and more compact. The FE-SEM images indicate that the WS_2 layers are well rearranged into structure of MoS_2 layers. The synergistic effect of high uniformity of MoS_2/WS_2 NF with small diameter (about 200–500 nm) could be the reason for the improvement of HER performance.

Figure 3 shows the TEM data of the synthesized MoS_2/WS_2 NF materials. Meanwhile, the TEM data of WS_2 NF and MoS_2 NF were provided in Figures S1 and S2, respectively. It is clear that the morphology of MoS_2/WS_2 NF elements is highly different from the morphologies of WS_2 NF and MoS_2 NF which are smaller and more porous. It could be interpreted that the different layers of WS_2 NF and MoS_2 NF could be mixed and disordered to form MoS_2/WS_2 NF. The d-spacing of catalysts is also calculated. The d-spacing of MoS_2/WS_2 NF is well similar to that of WS_2 NF and MoS_2 NF with 0.21 nm (006), 0.27 nm (110), and 0.64 nm (002). The SEAD images of MoS_2/WS_2 NF, WS_2 NF, and MoS_2 NF are also studied to confirm the lattice finger of the materials. The hazy-spotted SEAD pattern in Figure 3(c) indicates that the heterostructure of MoS_2 NF and WS_2 NF was formed. As can be seen from Figure S1(c), the bright spotted SEAD indicated the highly crystalline nature of WS_2 NF. Besides that, the hazy and broad diffraction ring of MoS_2 NF shows the low crystal quality of catalyst in Figure S2(c). The TEM-XDS data of MoS_2/WS_2 NF show the existence of Mo, W, and S elements while there are only W—S or Mo—S in WS_2 NF or MoS_2 NF. Besides that, the energy-dispersive spectroscopy (EDS) elemental mapping images of the sample, as shown in Figures 3(e), 3(f), 3(g), and 3(h), show the uniform distribution of Mo, W, and S elements. The TEM data include the successfully synthesized MoS_2/WS_2 NF, WS_2 NF, and MoS_2 NF materials.

The XPS measurements are also conducted to confirm the structure as well as the binding states of synthesized MoS_2/WS_2 NF, WS_2 NF, and MoS_2 NF materials. Figure 4(a) exhibits the wide XPS spectra of the prepared catalysts. It can be seen that there are Mo, W, and S elements that appeared in the XPS spectrum of MoS_2/WS_2 NF. There are only Mo and S or W and S elements that appeared in the spectrum of MoS_2 NF or the spectrum of WS_2 NF, respectively. The XPS data also confirmed the successful synthesis of MoS_2/WS_2 NF, WS_2 NF, and MoS_2 NF materials. To investigate the binding energy as well as the bonding structure of catalysts, the high-resolution XPS could be conducted. Figures 4(b), 4(c), 4(d), and 4(e) present the high-resolution fitted peaks of W 4f and Mo 3d in MoS_2/WS_2 NF, WS_2 NF, and MoS_2 NF, respectively. As can be seen from Figures 4(b) and 4(d), the W 4f peaks of MoS_2/WS_2 NF and WS_2 NF could be deconvoluted into four main peaks. The two peaks are located around 32.2 and 34.3 eV which could be assigned to the peaks of W—S bonding of W $4f_{7/2}$ and W $4f_{5/2}$, respectively. The two remaining peaks of WO_3 could be caused by the oxidation materials [47]. In Figures 4(c) and 4(e), the XPS spectrum of Mo 3d in MoS_2/WS_2 NF and MoS_2 NF could be fitted into four main peaks. There are two peaks of MoS_2 located at around 228.9 and 232 eV and two peaks of MoO_3 caused by the oxidation materials [48]. Interestingly, the peaks of nitrogen were observed in the synthesized catalysts. The in situ doped nitrogen in the prepared materials could be benefited for the catalytic properties of the catalysts [49, 50]. Figures S3, S4, and S5 present the high-resolution fitted peaks of S 2p and N 1s in MoS_2/WS_2 NF, WS_2 NF, and MoS_2 NF, respectively. The XPS peaks of S 2p in the synthesized materials is highly similarly, and they could be deconvoluted into S $2p_{3/2}$, S $2p_{1/2}$, and edge S located at around 161.8, 163.1, and 164.2 eV, respectively [51, 52].

The electronic modulation and the thermodynamic of the synthesized catalysts were completely investigated by ultraviolet photoemission spectroscopy (UPS) using Hel emission as light source ($h\nu = 21.2$ eV). The work function (WF) is the difference between the vacuum level and the Fermi level. The WF of the synthesized materials is a crucial parameter to evaluate the electrocatalytic activities of the materials because the WF could be calculated which could reveal the energy required to remove an electron from the surface of a catalysts. The WF of catalysts were extracted from the UPS spectra via the relationship between the incident photon energy ($h\nu$) and the secondary edge position (E_{SE}), as described in the following equation [53, 54]:

$$\mathrm{WF} = h\nu - \mathrm{E}_{SE} = 21.2 - \mathrm{E}_{SE}. \tag{18}$$

The UPS spectra and E_{SE} of the synthesized MoS_2/WS_2 NF, WS_2 NF, and MoS_2 NF were provided as Figures S6, S7, and S8, respectively. As shown and calculated in Figure 5(a), the WF of MoS_2/WS_2 NF, WS_2 NF, and MoS_2 NF were determined to be 3.1, 4.8, and 3.5 eV, respectively. As a result, the significant decrease in the WF of MoS_2/WS_2 NF could be attributed to the synergistic effect of MoS_2 and WS_2 elements

ijer, 2024, 1, Downloaded from https://onlinelibrary.wiley.com/doi/10.1155/2024/3192642 by Chung-Ang University, Wiley Online Library on [13/08/2024]. See the Terms and Conditions (https://onlinelibrary.wiley.com/terms-and-conditions) on Wiley Online Library for rules of use; OA articles are governed by the applicable Creative Commons License

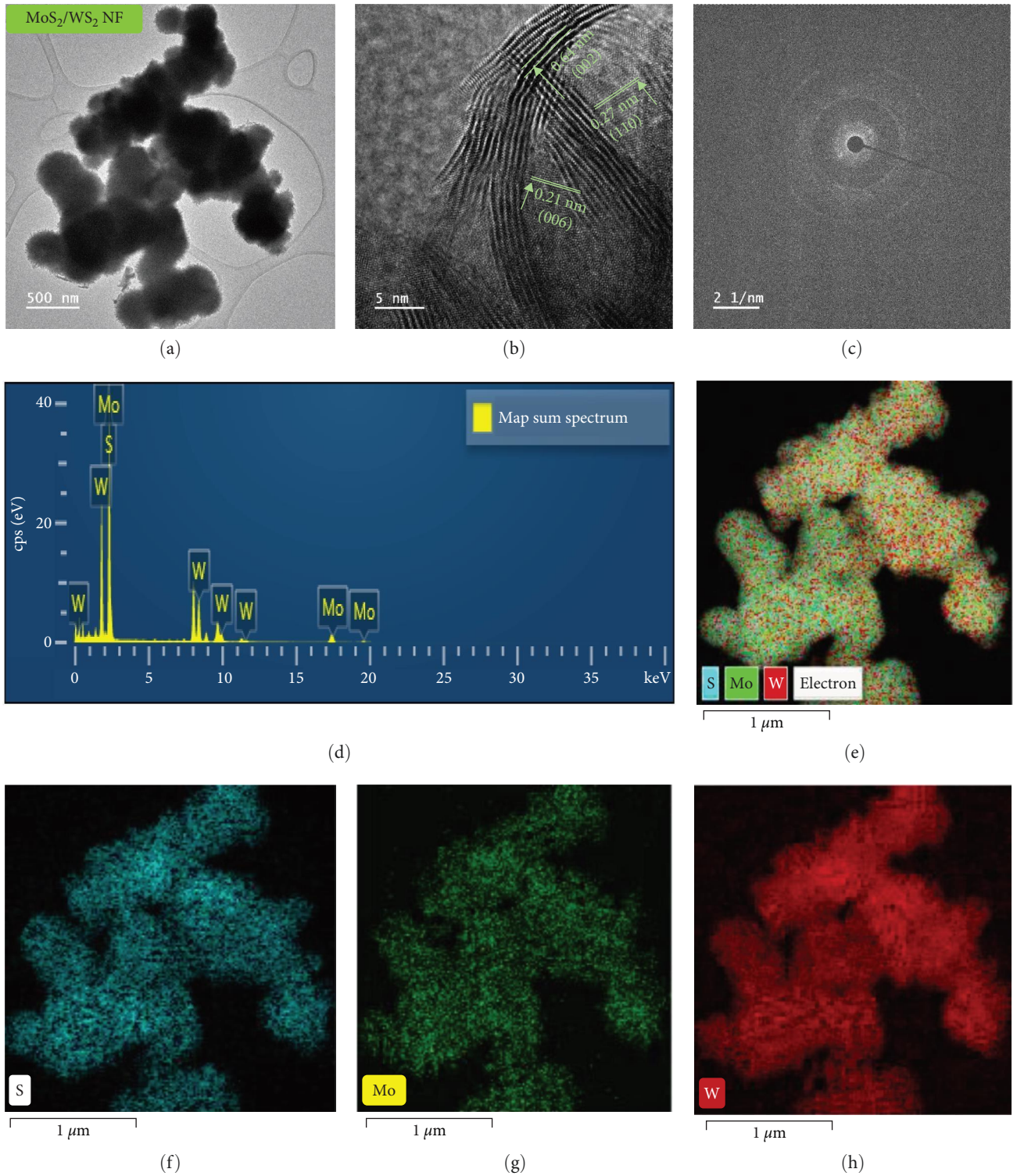
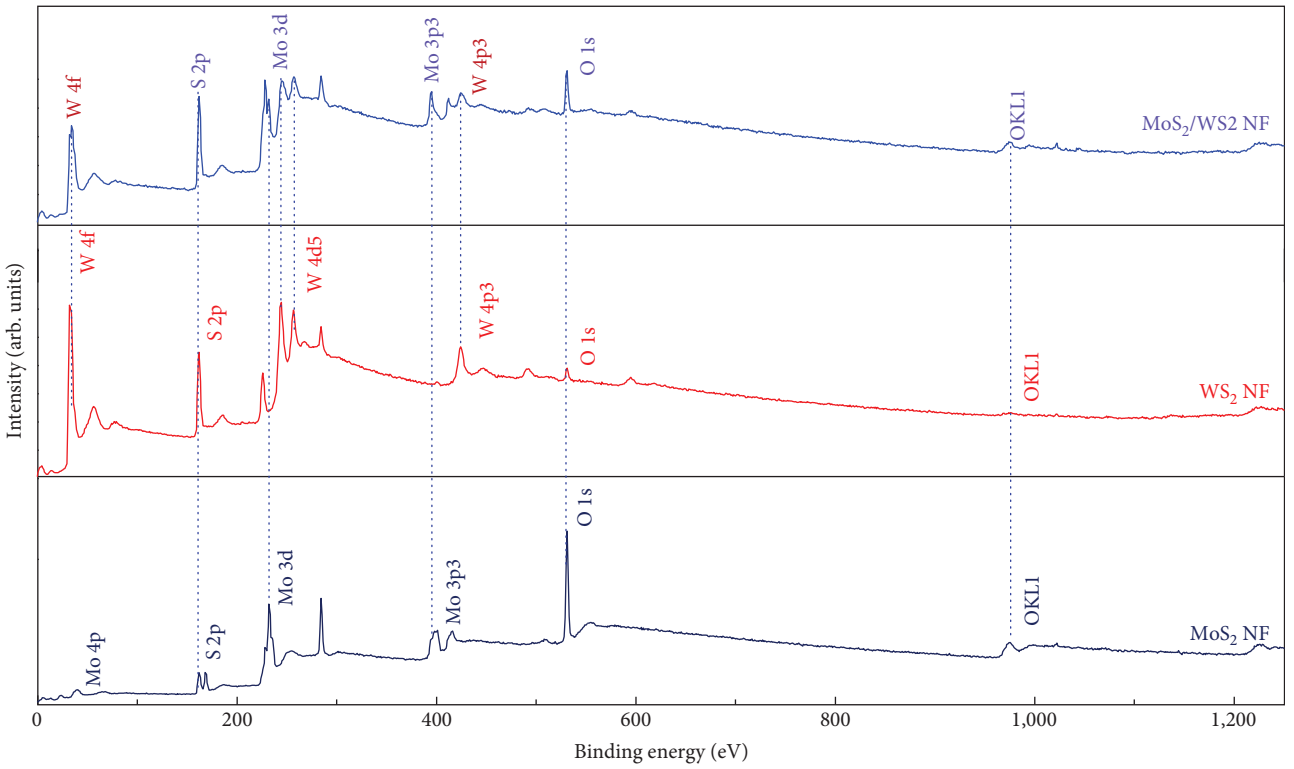


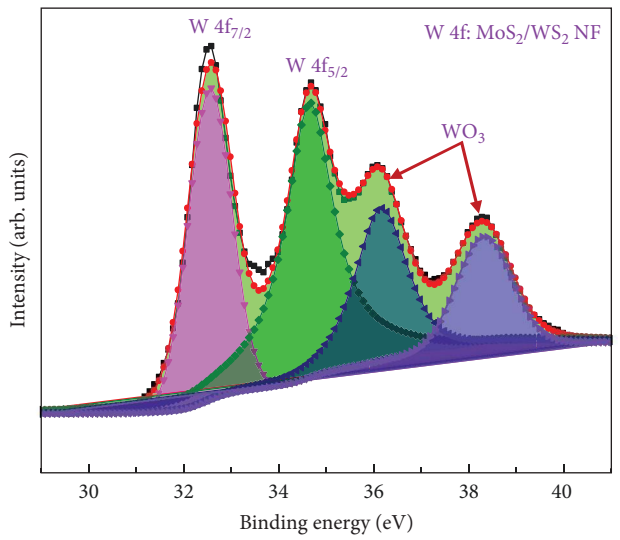
FIGURE 3: TEM data of MoS_2/WS_2 NF materials. (a) TEM images of MoS_2/WS_2 NF, (b) interlayer d-spacing of MoS_2/WS_2 NF, (c) SEAD image of MoS_2/WS_2 NF, (d) TEM-EDS of MoS_2/WS_2 NF, and (e–h) TEM mapping element contribution of MoS_2/WS_2 NF.

which is in line with the heterostructure between blue phosphorene and MoS_2 [55]. The results indicate that the heterostructures of MoS_2/WS_2 NF could be an effective approach in the modulation of the energy level. The decreased energy level could decrease the energy barrier for electron transfer which lead to the reducing of overpotential in HER process by enhancing the charge transfer between the layer and electrolyte [56, 57]. The HER performance could be evaluated by various factors including actives sites, conductivity, hydrogen binding energy, or stability of materials. Among them,

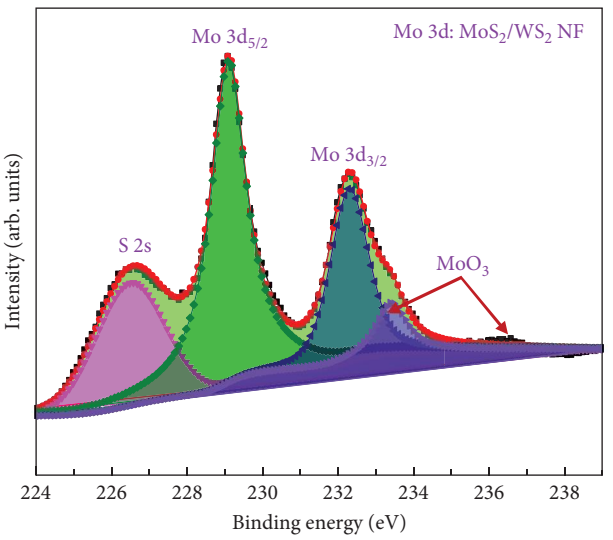
ijer, 2024, 1, Downloaded from https://onlinelibrary.wiley.com/doi/10.1155/2024/3192642 by Chung-Ang University, Wiley Online Library on [13/08/2024]. See the Terms and Conditions (https://onlinelibrary.wiley.com/terms-and-conditions) on Wiley Online Library for rules of use; OA articles are governed by the applicable Creative Commons License



(a)



(b)



(c)

Figure 4: Continued.

ijer, 2024, 1, Downloaded from https://onlinelibrary.wiley.com/doi/10.1155/2024/3192642 by Chung-Ang University, Wiley Online Library on [13/08/2024]. See the Terms and Conditions (https://onlinelibrary.wiley.com/terms-and-conditions) on Wiley Online Library for rules of use; OA articles are governed by the applicable Creative Commons License

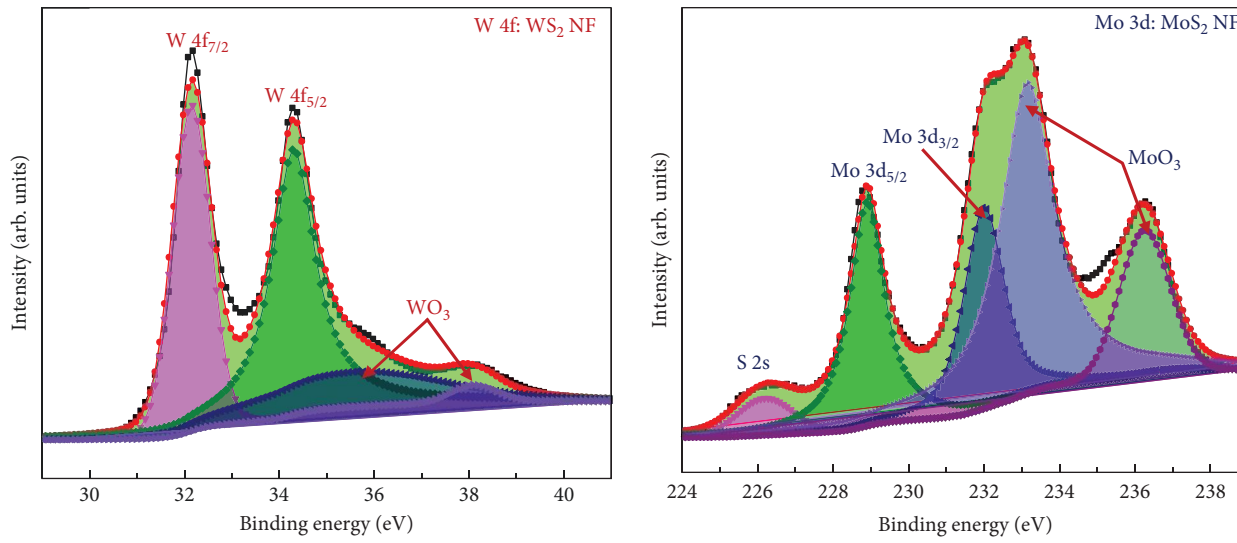


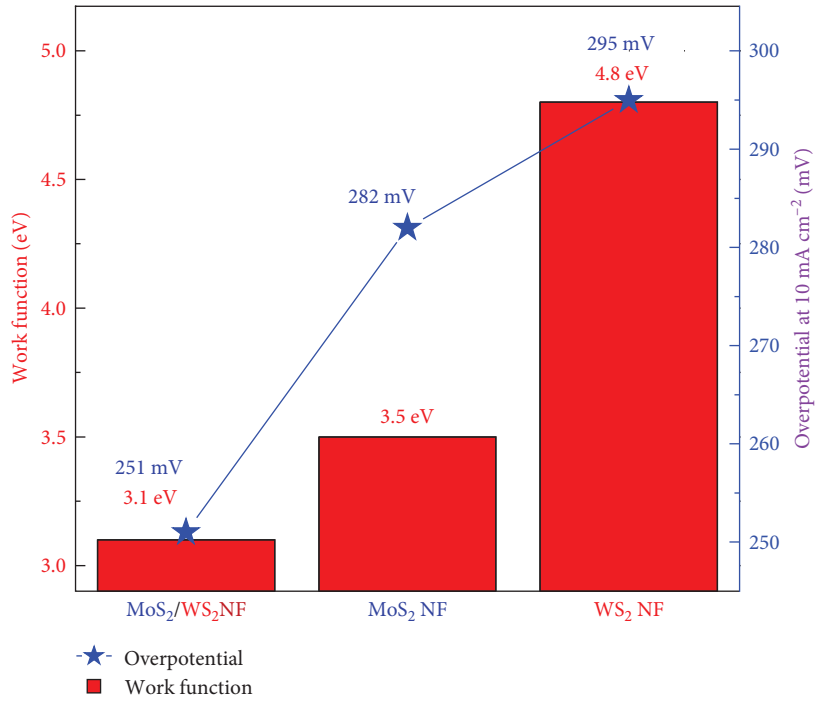
FIGURE 4: (a) XPS spectra of MoS_2/WS_2 NF, WS_2 NF, and MoS_2 NF materials and high-resolution HR XPS spectra of (b) W elements and (c) Mo elements in MoS_2/WS_2 NF and (d) W elements in WS_2 NF and (e) Mo elements in MoS_2 NF.

the enhancement of electron transfer is a good way to improve the catalytic activities of materials which is illustrated in Figure 5(b). The decrease of WF from UPS data confirms that the catalytic activities of MoS_2/WS_2 NF could be improved compared with that of WS_2 NF and MoS_2 NF which will be revealed in the next section.

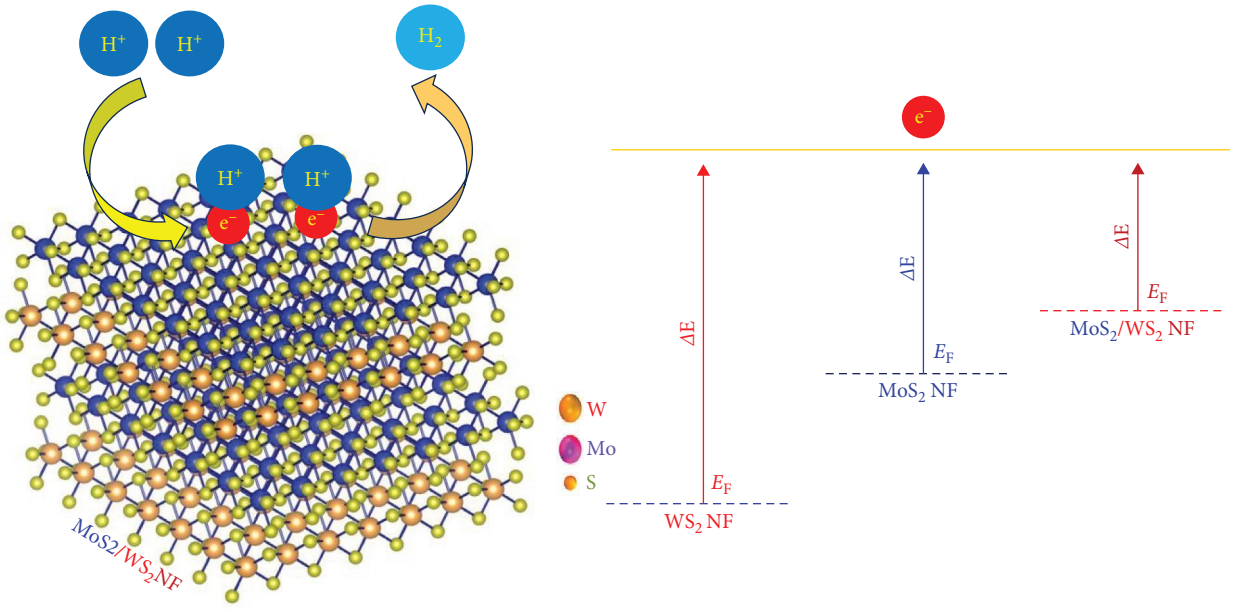
The pore size and pore volume of the catalyst also have an important influence on the HER performance. The larger pore size and pore volume of the catalyst could be facilitated for electrochemical hydrogen evolution process, in which the hydrogen gases could be formed and released from cathode electrode faster and more efficiently. The pore size and pore volume of the MoS_2/WS_2 NF, WS_2 NF, and MoS_2 NF materials were calculated by using the N_2 adsorption–desorption measurements. Figure 6(a) shows the pore size of the prepared materials; most of the pore sizes are distributed between 10 and 40 nm, indicating that the catalysts have a mesoporous structure. The large pore size of catalyst leads to the large total pore volume of the materials which could benefit for catalyst process. From the Table 2, the pore size of MoS_2/WS_2 NF (38.8 Å) is quite larger than that of WS_2 NF (25.295 Å) and MoS_2 NF (33.507 Å) materials that means the proton (H^+) could be easily attached to the surface electrode for reduced reaction and the formed gas (H_2) could be easily escape from surface electrode. The N_2 adsorption–desorption isotherms curves of MoS_2/WS_2 NF, WS_2 NF, and MoS_2 NF samples are shown in Figure 6(b). It can be seen that in the relatively high-pressure range of 0.85–1.0, the samples have a strong adsorption–desorption capacity, and all materials are isotherm type IV with H_3 hysteresis loops according to BDDT classification, which means all the samples show mesoporous properties and pore structure. In addition, the physical adsorption and desorption performance parameters of the samples are shown in Table 2. It presents that the pore volume of MoS_2/WS_2 NF is 0.0054 $cm^3\,g^{-1}$ which is significantly increased compared with that of WS_2 NF (0.002 $cm^3\,g^{-1}$) and MoS_2 NF (0.0035 $cm^3\,g^{-1}$). The pore volume of MoS_2/WS_2 NF is higher than that of the original WS_2 NF and MoS_2 NF which could be attributed to the disorder between MoS_2 and WS_2 layers in composite materials. The pore size and pore volume results indicated that the catalytic activities of MoS_2/WS_2 NF could be improved compared with that of WS_2 NF and MoS_2 NF [58, 59].

To evaluate the catalytic activity of the synthesized catalysts, the electrochemical performances of synthesized catalysts were completely investigated by various measurements to understand the performance improvements of MoS_2/WS_2 NF compared with that of WS_2 NF and MoS_2 NF. Figure 7 presents the electrocatalytic activities of the prepared materials. In Figure 7(a), the LSV curves of glassy carbon and Pt were also conducted to compare with that of synthesized catalysts. Overpotential is a very important descriptor to evaluate the activity of the electrocatalysts. Usually, the overpotential value corresponding to the current density of 10 mA cm^{-2} is used to compare the activities among different catalysts. As can be seen, there are significant changes of the prepared materials in the overpotential at 10 mA cm^{-2} which are 251, 295, and 282 mV for MoS_2/WS_2, WS_2 NF, and MoS_2 NF, respectively. Tafel slope is one of the most valuable parameters to evaluate the performance of the catalysts toward HER process which is related to the catalytic reaction mechanism in terms of electron-transfer kinetics. A material with smaller Tafel slope means that it is a better electrocatalyst because that leads to the faster electrocatalytic reaction kinetics. In Figure 7(b), it is clear that the Tafel slope of MoS_2/WS_2 NF (61 mV dec^{-1}) is highly decreased compared with that of WS_2 NF (89 mV dec^{-1}) and MoS_2 NF (81 mV dec^{-1}). The EIS of the synthesized materials are also measured to study the conductivity of catalysts. The equivalent circuit in the inset is composed of constant phase elements and charge–transfer resistances. As can be seen from Figure 7(c), the diameter semicircle of MoS_2/WS_2 NF is the smallest; it means that the conductivity of MoS_2/WS_2 NF is higher than that of MoS_2 NF and WS_2 NF. The EIS data demonstrated that the

ijer, 2024, 1, Downloaded from https://onlinelibrary.wiley.com/doi/10.1155/2024/3192642 by Chung-Ang University, Wiley Online Library on [13/08/2024]. See the Terms and Conditions (https://onlinelibrary.wiley.com/terms-and-conditions) on Wiley Online Library for rules of use; OA articles are governed by the applicable Creative Commons License



(a)



(b)

FIGURE 5: (a) The calculated WF of synthesized catalysts and overpotential at 10 mA cm^{-2} in HER measurements and (b) hydrogen evolution reaction mechanism and energy level modulation of prepared catalyst materials. ΔE represents overpotential and E_F represents the Fermi level.

electron conduction on the surface of the MoS_2/WS_2 NF is superior to that in the MoS_2 NF and WS_2 NF, which could be caused by the synergistic effect between MoS_2 and WS_2 layers in a heterostructure material. The double-layer capacitance (C_{dl}) of the prepared catalysts was also calculated by CV measurements at various scan rates. The CV curves of MoS_2/WS_2 NF, WS_2 NF, and MoS_2 NF at different scan rates were provided in Figures S9, S10, and S11, respectively. Figure 7(d) indicates that the C_{dl} of MoS_2/WS_2 NF (1.1 mF cm^{-2}) is almost twice that of WS_2 NF (0.63 mF cm^{-2}) and MoS_2 NF (0.68 mF cm^{-2}). After that, the electrochemical surface area (ECSA) of the synthesized catalysts were also calculated. The ECSA is a crucial factor to understand the effect between the active catalytic sites of the material and its activity, supporting catalysts comparison and benchmarking.

ijer, 2024, 1, Downloaded from https://onlinelibrary.wiley.com/doi/10.1155/2024/3192642 by Chung-Ang University, Wiley Online Library on [13/08/2024]. See the Terms and Conditions (https://onlinelibrary.wiley.com/terms-and-conditions) on Wiley Online Library for rules of use; OA articles are governed by the applicable Creative Commons License

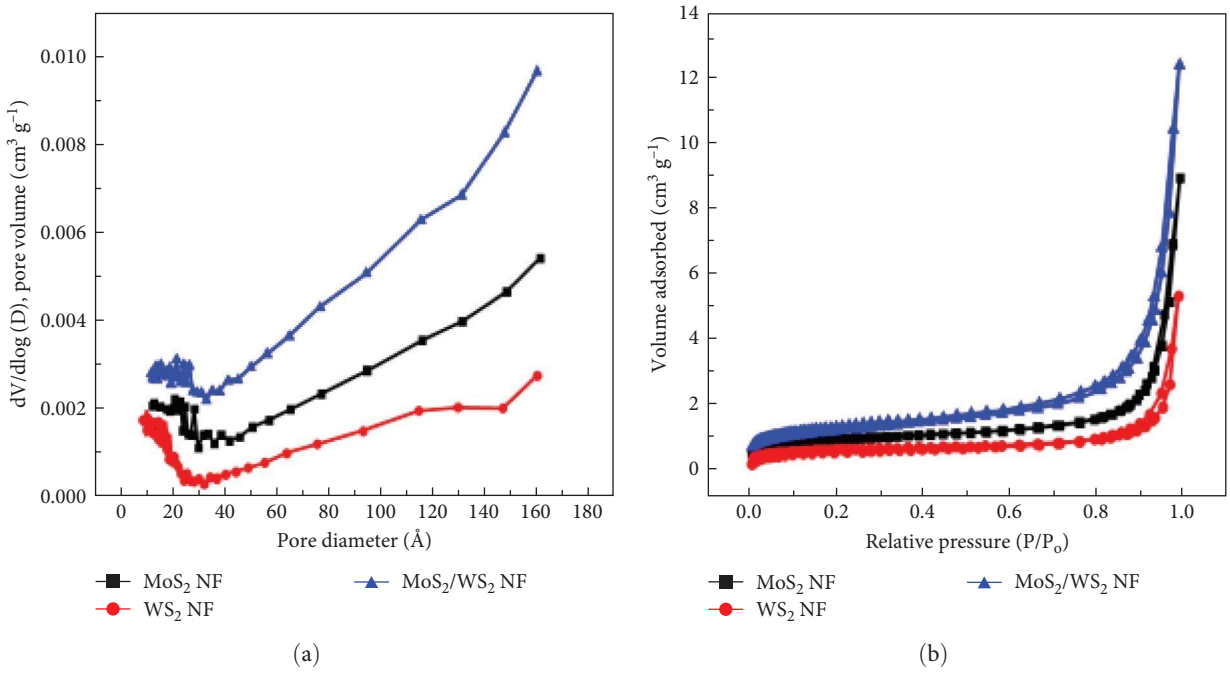


FIGURE 6: (a) The pore size distribution of the prepared catalysts and (b) nitrogen adsorption–desorption characterizations of MoS_2/WS_2 NF, WS_2 NF, and MoS_2 NF.

TABLE 2: Physical parameters of MoS_2/WS_2 NF, WS_2 NF, and MoS_2 NF.

Samples	S_{BET} ($m^2\,g^{-1}$)	Pore volume ($cm^3\,g^{-1}$)	Average pore size (Å)
MoS_2/WS_2 NF	3.72	0.0054	38.800
WS_2 NF	1.74	0.002	25.295
MoS_2 NF	2.78	0.0035	33.507

The ECSA can be calculated from the following equation [60, 61]:

$$\mathrm{ECSA} = \frac{C_{dl}}{C_s} = \frac{C_{dl}}{0.04} \tag{19}$$

where C_s is the capacitance of the sample of an atomically smooth planar surface of material per unit area under identical electrolyte conditions. Herein, the general specific capacitance of $C_s = 0.04\,\mathrm{mF\,cm^{-2}}$ could be employed. The results indicated that the ECSA of MoS_2/WS_2 NF, WS_2 NF, and MoS_2 NF are 27.5, 15.75, and 17, respectively.

When hydrolysis process takes place, the hydrogen gas is freed from the surface of cathode electrode. The protons (H^+) in the electrolyte could receive electrons from the electrode under an applied voltage. The HER mechanism in acidic media could be reacted as the following equations:

$$\begin{aligned} &H^+ + e^- = H_{ad} && \textit{Volmer step} \\ &H^+ + e^- + H_{ad} && \textit{H}_2\ \textit{Heyrovsky step} \\ &H_{ad} + H_{ad} = H_2 && \textit{Tafel step} \end{aligned} \tag{20}$$

The yield of the released hydrogen gas is highly dependent on the properties of the cathode electrode materials. If the cathode electrode is made from highly active catalysts with a larger specific area, the hydrogen gas will be more easily formed and released leading to high yield product. Figure 7(e) shows the specific surface area (S_{BET}) of MoS_2/WS_2 NF ($3.72\,m^2\,g^{-1}$) which is higher than that of WS_2 NF ($1.74\,m^2\,g^{-1}$) and MoS_2 ($2.78\,\mathrm{NF\,m^2\,g^{-1}}$). The larger S_{BET} induces to the better HER performance of MoS_2/WS_2 NF compared with that of WS_2 NF and MoS_2 NF which have been indicated by overpotential and Tafel slope value.

The stability of the electrocatalysts is another important parameter to determine the properties of the materials. For HER performance, the stability of MoS_2/WS_2 NF was continuously tested by CV and CA measurements. The CV and CA results were presented in Figures S12 and S13, respectively. As can be seen, in both CV and CA curves, there is a neglectable degradation for 1,000 cycles of CV test and 12 hr of CA test. After stability tests, the LSV of MoS_2/WS_2 NF was also reconducted to investigate the degradation of the catalyst. In Figure 7(f), the small change of LSV curves before and after stability tests indicates the superior stability of the catalysts toward HER application. All the data confirm that the HER performance improvement of MoS_2/WS_2 NF compared with that of WS_2 NF and MoS_2 NF could be contributed to the larger specific area, good conductivity, and synergistic effect of the heterostructure materials. Therefore, MoS_2/WS_2

ijer, 2024, 1, Downloaded from https://onlinelibrary.wiley.com/doi/10.1155/2024/3192642 by Chung-Ang University, Wiley Online Library on [13/08/2024]. See the Terms and Conditions (https://onlinelibrary.wiley.com/terms-and-conditions) on Wiley Online Library for rules of use; OA articles are governed by the applicable Creative Commons License

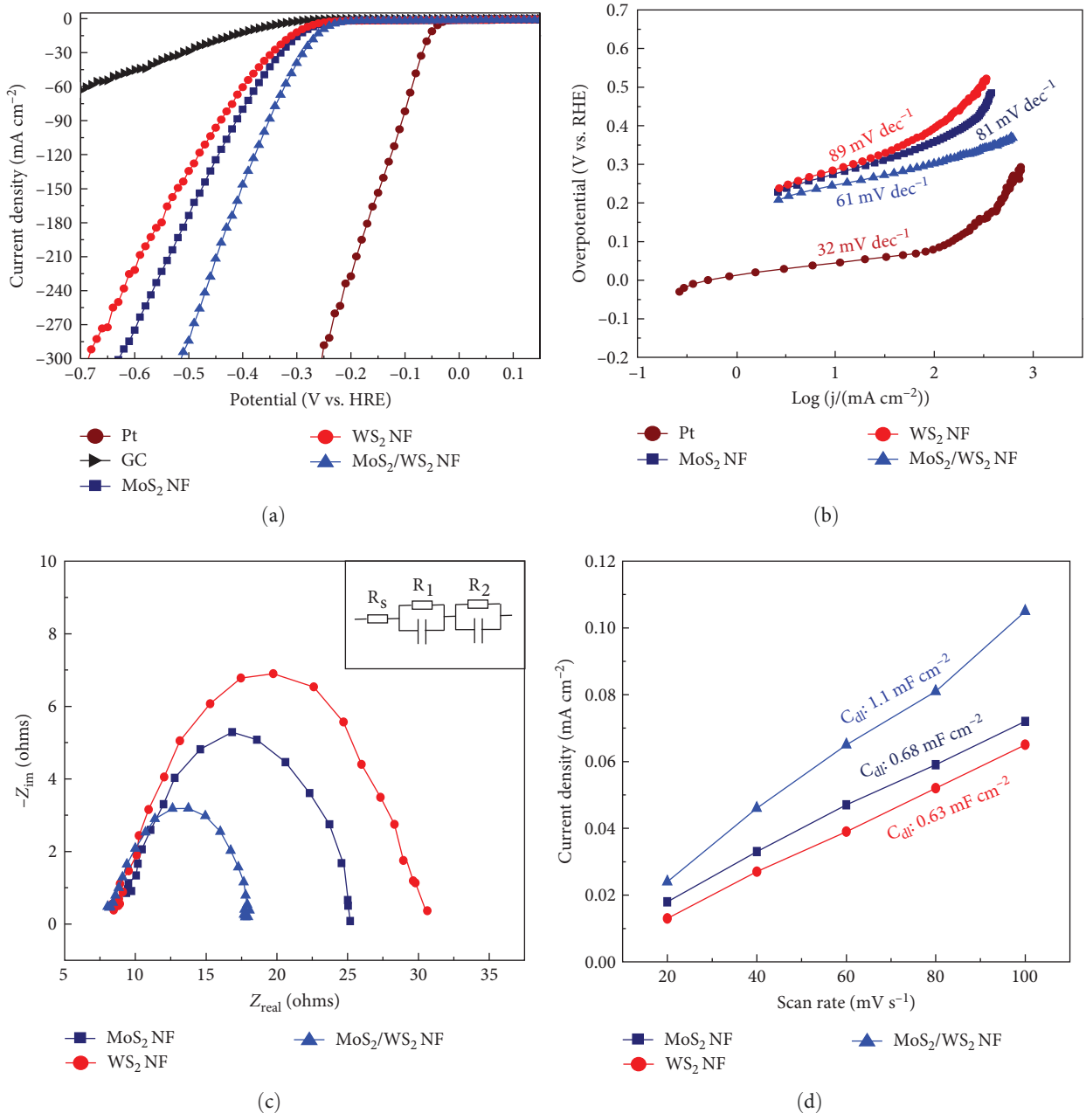


Figure 7: Continued.

ijer, 2024, 1, Downloaded from https://onlinelibrary.wiley.com/doi/10.1155/2024/3192642 by Chung-Ang University, Wiley Online Library on [13/08/2024]. See the Terms and Conditions (https://onlinelibrary.wiley.com/terms-and-conditions) on Wiley Online Library for rules of use; OA articles are governed by the applicable Creative Commons License

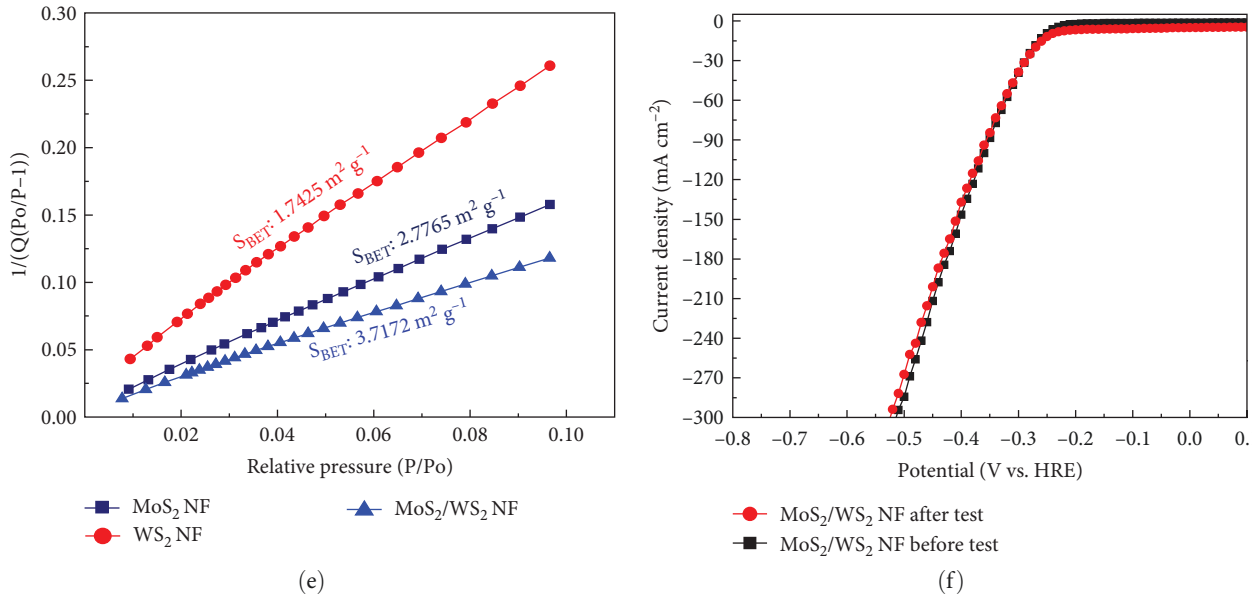


FIGURE 7: HER performance of the synthesized catalysts: (a) LSV curves of MoS_2/WS_2 NF, WS_2 NF, and MoS_2 NF, (b) calculated Tafel slope of the synthesized catalysts, (c) EIS curves of the prepared catalysts, (d) Calculated C_{dl} of the prepared catalysts, (e) S_{BET} of the prepared catalysts, and (f) LSV curves of MoS_2/WS_2 NF before and after stability tests.

NF could be a great catalyst for electrochemical application including HER process.

4. Conclusions

In summary, various nanoflower catalysts have been successfully prepared including MoS_2/WS_2 NF, WS_2 NF, and MoS_2 NF. Their structures, morphologies, and catalytic activities were also completely investigated and confirmed. The results indicate that MoS_2/WS_2 NF exhibits great performance toward HER application with low overpotential (251 mV at current density of 10 mA cm^{-2}) and small Tafel slope (61 mV dec^{-1}) as well as the superior stability in acidic media. The catalytic improvements of MoS_2/WS_2 NF could be assigned to the high uniformity of small nanoflower (200–500 nm) and large surface area as well as the synergistic effect of MoS_2 and WS_2 elements. The study has provided a facile process to prepare a good catalytic material for high-efficient hydrogen products as well as other electrocatalytic processes.

Data Availability

Data will be made available on request.

Conflicts of Interest

The authors declare that they have no known competing financial interests or personal relationships that could have appeared to influence the work presented in this manuscript.

Authors' Contributions

Tuan Van Nguyen is responsible for the conceptualization, investigation, and writing—original draft. Mahider Asmare Tekalgne is responsible for the conceptualization, investigation, and writing—original draft. Quyet Van Le is responsible for the conceptualization and investigation. Thang Phan Nguyen is responsible for the conceptualization and investigation. Vandung Dao is responsible for the conceptualization. Chau Van Tran is responsible for the conceptualization. Sang Hyun Ahn is responsible for the supervision and writing—review and editing. Soo Young Kim is responsible for the project administration, supervision, and writing—review and editing. Tuan Van Nguyen and Mahider Tekalgne contributed equally to this work.

Acknowledgments

This research was supported by the NRF funded by the Korean government (2022M3H4A1A01012712 and 2022M 3H4A1A04096380).

Supplementary Materials

Figure S1: the TEM data of WS_2 NF material. Figure S2: the TEM data of MoS_2 NF material. Figure S3: the HR XPS spectra of (a) S 2p and (b) N 1s in MoS_2/WS_2 NF material. Figure S4: the HR XPS spectra of (a) S 2p and (b) N 1s in WS_2 NF material. Figure S5: the HR XPS spectra of (a) S 2p and (b) N 1s in MoS_2 NF material. Figure S6: the UPS spectrum of MoS_2/WS_2 NF. Figure S7: the UPS spectrum of WS_2 NF. Figure S8: the UPS spectrum of MoS_2 NF. Figure S9: the CV of MoS_2/WS_2 NF at different scan rates. Figure S10: the CV of WS_2 NF at different scan rates. Figure S11: the CV of MoS_2 NF at different scan rates. Figure S12: the stability of MoS_2/WS_2 NF tested by CV measurements. Figure S13: the stability of MoS_2/WS_2 NF tested by CA measurements. (*Supplementary Materials*)

ijer, 2024, 1, Downloaded from https://onlinelibrary.wiley.com/doi/10.1155/2024/3192642 by Chung-Ang University, Wiley Online Library on [13/08/2024]. See the Terms and Conditions (https://onlinelibrary.wiley.com/terms-and-conditions) on Wiley Online Library for rules of use; OA articles are governed by the applicable Creative Commons License

References

[1] K. A. Huynh, S. R. Bae, T. V. Nguyen et al., "Ligand-assisted sulfide surface treatment of $CsPbI_3$ perovskite quantum dots to increase photoluminescence and recovery," *ACS Photonics*, vol. 8, pp. 1979–1987, 2021.

[2] K. A. Huynh, T. Van Nguyen, S. R. Bae et al., "Surface treatment of mixed-halide $CsPb(Br_xI_{1-x})_3$ perovskite quantum dots for thermal stability enhancement," *Materials Research Bulletin*, vol. 146, Article ID 111622, 2022.

[3] T. P. Nguyen, D. L. T. Nguyen, V. H. Nguyen et al., "Recent advances in TiO_2-based photocatalysts for reduction of CO_2 to fuels," *Nanomaterials*, vol. 10, Article ID 337, 2020.

[4] S. Bae, S. Lee, H. Ryu, and W. J. Lee, "Improvement of photoelectrochemical properties of CuO photoelectrode by Li doping," *Korean Journal of Metals and Materials*, vol. 60, pp. 577–586, 2022.

[5] S. A. Lee, J. W. Yang, T. H. Lee et al., "Multifunctional nano-heterogeneous $Ni(OH)_2$/NiFe catalysts on silicon photoanode toward efficient water and urea oxidation," *Applied Catalysis B: Environmental*, vol. 317, Article ID 121765, 2022.

[6] M. G. Lee, J. W. Yang, H. Park et al., "Crystal facet engineering of TiO_2 nanostructures for enhancing photoelectrochemical water splitting with $BiVO_4$ nanodots," *Nano-Micro Letters*, vol. 14, no. 1, Article ID 48, 2022.

[7] S. Kim, K. H. Kim, C. Oh, K. Zhang, and J. H. Park, "Artificial photosynthesis for high-value-added chemicals: old material, new opportunity," *Carbon Energy*, vol. 4, pp. 21–44, 2022.

[8] K. H. Kim, C. W. Choi, S. Choung et al., "Continuous oxygen vacancy gradient in TiO_2 photoelectrodes by a photoelectrochemical-driven, self-purification, process," *Advanced Energy Materials*, vol. 12, Article ID 2103495, 2022.

[9] J. H. Cho, C. Lee, S. H. Hong et al., "Transition metal ion doping on ZIF-8 enhances the electrochemical CO_2 reduction reaction," *Advanced Materials*, vol. 35, Article ID 2208224, 2023.

[10] T. Van Nguyen, H. H. Do, T. Q. Trung et al., "Stable and multicolored electrochromic device based on polyaniline-tungsten oxide hybrid thin film," *Journal of Alloys and Compounds*, vol. 882, Article ID 160718, 2021.

[11] B. Jin, Y. Cho, C. Park et al., "A two-photon tandem black phosphorus quantum dot-sensitized $BiVO_4$ photoanode for solar water splitting," *Energy & Environmental Science*, vol. 15, pp. 672–679, 2022.

[12] M. K. Lee, M. Shokouhimehr, S. Y. Kim, and H. W. Jang, "Two-dimensional metal-organic frameworks and covalent-organic frameworks for electrocatalysis: distinct merits by the reduced dimension," *Advanced Energy Materials*, vol. 12, Article ID 2003990, 2022.

[13] T. Van Nguyen, T. P. Nguyen, Q. Van Le, D. Van Dao, S. H. Ahn, and S. Y. Kim, "Synthesis of very small molybdenum disulfide nanoflowers for hydrogen evolution reaction," *Applied Surface Science*, vol. 607, Article ID 154979, 2023.

[14] A. Kumar, I. H. Kim, L. Mathur, H. S. Kim, and S. J. Song, "Design of tin polyphosphate for hydrogen evolution reaction and supercapacitor applications," *Journal of the Korean Ceramic Society*, vol. 58, pp. 688–699, 2021.

[15] P. J. Megía, A. J. Vizcaíno, J. A. Calles, and A. Carrero, "Hydrogen production technologies: from fossil fuels toward renewable sources. A mini review," *Energy & Fuels*, vol. 35, no. 2, pp. 16403–16415, 2021.

[16] V. H. Nguyen, B. S. Nguyen, Z. Jin et al., "Towards artificial photosynthesis: sustainable hydrogen utilization for photocatalytic reduction of CO_2 to high-value renewable fuels," *Chemical Engineering Journal*, vol. 402, Article ID 126184, 2020.

[17] V. Kumar, R. K. Mishra, L. G. Trung et al., "Copper, palladium, and reduced graphene oxide Co-doped layered WS_2/WO_3 nanostructures for electrocatalytic hydrogen generation," *Electronic Materials Letters*, vol. 20, pp. 414–424, 2023.

[18] M. A. Tekalgne, H. H. Do, T. V. Nguyen et al., "Efficient electrocatalysts for hydrogen evolution reaction using heteroatom-doped mxene nanosheet," *International Journal of Energy Research*, vol. 2023, Article ID 8980888, 11 pages, 2023.

[19] D. Van Dao, G. Di Liberto, H. Ko et al., "$LaFeO_3$ meets nitrogen-doped graphene functionalized with ultralow Pt loading in an impactful Z-scheme platform for photocatalytic hydrogen evolution," *Journal of Materials Chemistry A*, vol. 10, pp. 3330–3340, 2022.

[20] C. M. Kai, C. Kong, F. J. Zhang, D. C. Li, Y. R. Wang, and W. C. Oh, "In situ growth of CdS spherical nanoparticles/Ti_3C_2 MXene nanosheet heterojunction with enhanced photocatalytic hydrogen evolution," *Journal of the Korean Ceramic Society*, vol. 59, pp. 302–311, 2022.

[21] H. H. Do, D. L. T. Nguyen, X. C. Nguyen et al., "Recent progress in TiO_2-based photocatalysts for hydrogen evolution reaction: a review," *Arabian Journal of Chemistry*, vol. 13, pp. 3653–3671, 2020.

[22] V.-H. Nguyen, B.-S. Nguyen, C. Hu et al., "Novel architecture titanium carbide ($Ti_3C_2T_x$) MXene cocatalysts toward photocatalytic hydrogen production: a mini-review," *Nanomaterials*, vol. 10, no. 4, Article ID 602, 2020.

[23] J. N. Hansen, H. Prats, K. K. Toudahl et al., "Is there anything better than Pt for HER?" *ACS Energy Letters*, vol. 6, pp. 1175–1180, 2021.

[24] S. Wang, A. Lu, and C.-J. Zhong, "Hydrogen production from water electrolysis: role of catalysts," *Nano Convergence*, vol. 8, no. 1, Article ID 4, 2021.

[25] Z. Cui, W. Jiao, Z. Huang et al., "Design and synthesis of noble metal-based alloy electrocatalysts and their application in hydrogen evolution reaction," *Small*, vol. 19, Article ID 2301465, 2023.

[26] H. Wu, C. Feng, L. Zhang, J. Zhang, and D. P. Wilkinson, "Non-noble metal electrocatalysts for the hydrogen evolution reaction in water electrolysis," *Electrochemical Energy Reviews*, vol. 4, pp. 473–507, 2021.

[27] L. Yu, Q. Zhu, S. Song et al., "Non-noble metal-nitride based electrocatalysts for high-performance alkaline seawater electrolysis," *Nature Communications*, vol. 10, no. 1, Article ID 5106, 2019.

[28] C. Wang, H. Shang, H. Xu, and Y. Du, "Nanoboxes endow non-noble-metal-based electrocatalysts with high efficiency for overall water splitting," *Journal of Materials Chemistry A*, vol. 9, pp. 857–874, 2021.

[29] C. Liu, C. Kong, F. J. Zhang et al., "Research progress of defective MoS_2 for photocatalytic hydrogen evolution," *Journal of the Korean Ceramic Society*, vol. 58, pp. 135–147, 2021.

[30] T. Van Nguyen, M. Tekalgne, T. P. Nguyen, Q. Van Le, S. H. Ahn, and S. Y. Kim, "Electrocatalysts based on MoS2 and WS2 for hydrogen evolution reaction: an overview," *Battery Energy*, vol. 2, Article ID 20220057, 2023.

[31] T. Van Nguyen, H. H. Do, M. Tekalgne et al., "WS_2–WC-WO_3 nano-hollow spheres as an efficient and durable catalyst for hydrogen evolution reaction," *Nano Convergence*, vol. 8, no. 1, pp. 1–12, 2021.

[32] G. Li, D. Zhang, Q. Qiao et al., "All the catalytic active sites of MoS_2 for hydrogen evolution," *Journal of the American Chemical Society*, vol. 138, no. 51, pp. 16632–16638, 2016.

ijer, 2024, 1, Downloaded from https://onlinelibrary.wiley.com/doi/10.1155/2024/3192642 by Chung-Ang University, Wiley Online Library on [13/08/2024]. See the Terms and Conditions (https://onlinelibrary.wiley.com/terms-and-conditions) on Wiley Online Library for rules of use; OA articles are governed by the applicable Creative Commons License

[33] T. V. Nguyen, Q. V. Le, C. C. Nguyen et al., "Synthesis of nano-coral tungsten carbide/carbon fibers as efficient catalysts for hydrogen evolution reaction," *International Journal of Energy Research*, vol. 46, pp. 13089–13098, 2022.

[34] T. Van Nguyen, M. Tekalgne, T. P. Nguyen et al., "Control of the morphologies of molybdenum disulfide for hydrogen evolution reaction," *International Journal of Energy Research*, vol. 46, pp. 11479–11491, 2022.

[35] T. Van Nguyen, T. P. Nguyen, Q. Van Le, D. Van Dao, S. H. Ahn, and S. Y. Kim, "Facile route for synthesizing WS_2/W_2C nano hollow flowers and their application for hydrogen evolution reaction," *Journal of Alloys and Compounds*, vol. 955, Article ID 170231, 2023.

[36] Y. Chen and M. Sun, "Two-dimensional WS_2/MoS_2 heterostructures: properties and applications," *Nanoscale*, vol. 13, pp. 5594–5619, 2021.

[37] Y. Gong, J. Lin, X. Wang et al., "Vertical and in-plane heterostructures from WS_2/MoS_2 monolayers," *Nature Materials*, vol. 13, no. 12, pp. 1135–1142, 2014.

[38] H. J. Lee, S. W. Lee, H. Hwang, S. I. Yoon, Z. Lee, and H. S. Shin, "Vertically oriented MoS_2/WS_2 heterostructures on reduced graphene oxide sheets as electrocatalysts for hydrogen evolution reaction," *Materials Chemistry Frontiers*, vol. 5, pp. 3396–3403, 2021.

[39] X. Hong, J. Kim, S.-F. Shi et al., "Ultrafast charge transfer in atomically thin MoS_2/WS_2 heterostructures," *Nature Nanotechnology*, vol. 9, no. 9, pp. 682–686, 2014.

[40] S. Hu, W. Chen, J. Zhou et al., "Preparation of carbon coated MoS_2 flower-like nanostructure with self-assembled nanosheets as high-performance lithium-ion battery anodes," *Journal of Materials Chemistry A*, vol. 2, pp. 7862–7872, 2014.

[41] C. S. Rout, P. D. Joshi, R. V. Kashid et al., "Superior field emission properties of layered WS_2-RGO nanocomposites," *Scientific Reports*, vol. 3, Article ID 3282, 2013.

[42] M. A. Koklioti, C. Bittencourt, X. Noirfalise, I. Saucedo-Orozco, M. Quintana, and N. Tagmatarchis, "Nitrogen-doped silver-nanoparticle-decorated transition-metal dichalcogenides as surface-enhanced Raman scattering substrates for sensing polycyclic aromatic hydrocarbons," *ACS Applied Nano Materials*, vol. 1, pp. 3625–3635, 2018.

[43] X. Tong, Y. Qi, J. Chen, N. Wang, and Q. Xu, "Supercritical CO_2-assisted reverse-micelle-induced solution-phase fabrication of two-dimensional metallic 1T-MoS_2 and 1T-WS_2," *ChemNanoMat*, vol. 3, pp. 466–471, 2017.

[44] A. Berkdemir, H. R. Gutiérrez, A. R. Botello-Méndez et al., "Identification of individual and few layers of WS_2 using Raman spectroscopy," *Scientific Reports*, vol. 3, Article ID 1755, 2013.

[45] W. Zhao, Z. Ghorannevis, K. K. Amara et al., "Lattice dynamics in mono-and few-layer sheets of WS_2 and WSe_2," *Nanoscale*, vol. 5, no. 20, pp. 9677–9683, 2013.

[46] H. Seok, Y. T. Megra, C. K. Kanade et al., "Low-temperature synthesis of wafer-scale MoS_2–WS_2 vertical heterostructures by single-step penetrative plasma sulfurization," *ACS Nano*, vol. 15, pp. 707–718, 2021.

[47] F. Reale, P. Palczynski, I. Amit et al., "High-mobility and high-optical quality atomically thin WS_2," *Scientific Reports*, vol. 7, Article ID 14911, 2017.

[48] Y. T. Ho, C. H. Ma, T. T. Luong et al., "Layered MoS_2 grown on c-sapphire by pulsed laser deposition," *Physica Status Solidi (RRL)—Rapid Research Letters*, vol. 9, pp. 187–191, 2015.

[49] R. Li, L. Yang, T. Xiong et al., "Nitrogen doped MoS_2 nanosheets synthesized via a low-temperature process as electrocatalysts with enhanced activity for hydrogen evolution reaction," *Journal of Power Sources*, vol. 356, pp. 133–139, 2017.

[50] D. Liu, Z. Lv, J. Dang et al., "Nitrogen-doped MoS_2/Ti_3C_2T X heterostructures as ultra-efficient alkaline her electrocatalysts," *Inorganic Chemistry*, vol. 60, pp. 9932–9940, 2021.

[51] S. Lu, W. Luo, Z. Chao, Y. Liu, S. Han, and J. Fan, "A novel honeycomb-like WS_{2-x}/CoS@C composite as anode for lithium ion batteries," *Journal of Materials Science*, vol. 57, pp. 5118–5129, 2022.

[52] C. Backes, R. J. Smith, N. McEvoy et al., "Edge and confinement effects allow in situ measurement of size and thickness of liquid-exfoliated nanosheets," *Nature Communications*, vol. 5, Article ID 4576, 2014.

[53] G. H. Kim, H. B. Kim, B. Walker et al., "Effects of ionic liquid molecules in hybrid PbS quantum dot-organic solar cells," *ACS Applied Materials & Interfaces*, vol. 5, pp. 1757–1760, 2013.

[54] L. Zhai, X. She, L. Zhuang et al., "Modulating built-in electric field via variable oxygen affinity for robust hydrogen evolution reaction in neutral media," *Angewandte Chemie*, vol. 134, Article ID e202116057, 2022.

[55] Q. Peng, Z. Wang, B. Sa, B. Wu, and Z. Sun, "Electronic structures and enhanced optical properties of blue phosphorene/transition metal dichalcogenides van der Waals heterostructures," *Scientific Reports*, vol. 6, Article ID 31994, 2016.

[56] Y. Shi, Y. Zhou, D.-R. Yang et al., "Energy level engineering of MoS_2 by transition-metal doping for accelerating hydrogen evolution reaction," *Journal of the American Chemical Society*, vol. 139, no. 43, pp. 15479–15485, 2017.

[57] M. Li, B. Cai, R. Tian et al., "Vanadium doped 1T MoS_2 nanosheets for highly efficient electrocatalytic hydrogen evolution in both acidic and alkaline solutions," *Chemical Engineering Journal*, vol. 409, Article ID 128158, 2021.

[58] D. Xiang, X. Hao, and Z. Jin, "Cu/CdS/MnO_x nanostructure-based photocatalyst for photocatalytic hydrogen evolution," *ACS Applied Nano Materials*, vol. 4, pp. 13848–13860, 2021.

[59] Y. Quan, G. Wang, J. Li, and Z. Jin, "Enhanced effect of CdS on amorphous $Mo_{15}S_{19}$ for photocatalytic hydrogen evolution," *New Journal of Chemistry*, vol. 45, pp. 3920–3931, 2021.

[60] C. Wang, H. Lu, K. Tang et al., "Atom removal on the basal plane of layered MoS_2 leading to extraordinarily enhanced electrocatalytic performance," *Electrochimica Acta*, vol. 336, Article ID 135740, 2020.

[61] J. Hu, C. Zhang, L. Jiang et al., "Nanohybridization of MoS_2 with layered double hydroxides efficiently synergizes the hydrogen evolution in alkaline media," *Joule*, vol. 1, pp. 383–393, 2017.

ijer, 2024, 1, Downloaded from https://onlinelibrary.wiley.com/doi/10.1155/2024/3192642 by Chung-Ang University, Wiley Online Library on [13/08/2024]. See the Terms and Conditions (https://onlinelibrary.wiley.com/terms-and-conditions) on Wiley Online Library for rules of use; OA articles are governed by the applicable Creative Commons License